Relaxation and Prethermalization in an Isolated Quantum System

M. Gring,[1] M. Kuhnert,[1] T. Langen,[1] T. Kitagawa,[2] B. Rauer,[1] M. Schreitl,[1] I. Mazets,[1,3] D. Adu Smith,[1] E. Demler,[2] J. Schmiedmayer[1,4]*

Understanding relaxation processes is an important unsolved problem in many areas of physics. A key challenge is the scarcity of experimental tools for the characterization of complex transient states. We used measurements of full quantum mechanical probability distributions of matter-wave interference to study the relaxation dynamics of a coherently split one-dimensional Bose gas and obtained comprehensive information about the dynamical states of the system. After an initial rapid evolution, the full distributions reveal the approach toward a thermal-like steady state characterized by an effective temperature that is independent from the initial equilibrium temperature of the system before the splitting process. We conjecture that this state can be described through a generalized Gibbs ensemble and associate it with prethermalization.

Despite its fundamental importance, a general understanding of how isolated quantum many-body systems approach thermal equilibrium is still elusive. Theoretical concepts such as the quantum ergodic theory or the eigenstate thermalization hypothesis (*1*–*3*) infer requirements for a system to be able to undergo relaxation, but it is still unclear on what time scale this occurs. In situations in which conservation laws inhibit efficient relaxation, many-body systems are expected to display a complex behavior. An intriguing phenomenon that has been suggested in this context is prethermalization (*4*), a general concept that is predicted to be applicable to a large variety of physical systems (*5*–*9*). In the present understanding, prethermalization is characterized by the rapid establishment of a quasi-stationary state that already exhibits some equilibrium-like properties. Full relaxation to the

[1]Vienna Center for Quantum Science and Technology, Atominstitut, Technische Universität (TU) Wien, Stadionallee 2, 1020 Vienna, Austria. [2]Harvard–Massachussets Institute of Technology Center for Ultracold Atoms (CUA), Department of Physics, Harvard University, Cambridge, MA 02138, USA. [3]Ioffe Physico-Technical Institute of the Russian Academy of Science, 194021 St. Petersburg, Russia. [4]Zentrum für Mikro- und Nanostrukturen (ZMNS), TU Wien, Floragasse 7, 1040 Vienna, Austria.

*To whom correspondence should be addressed. E-mail: schmiedmayer@atomchip.org

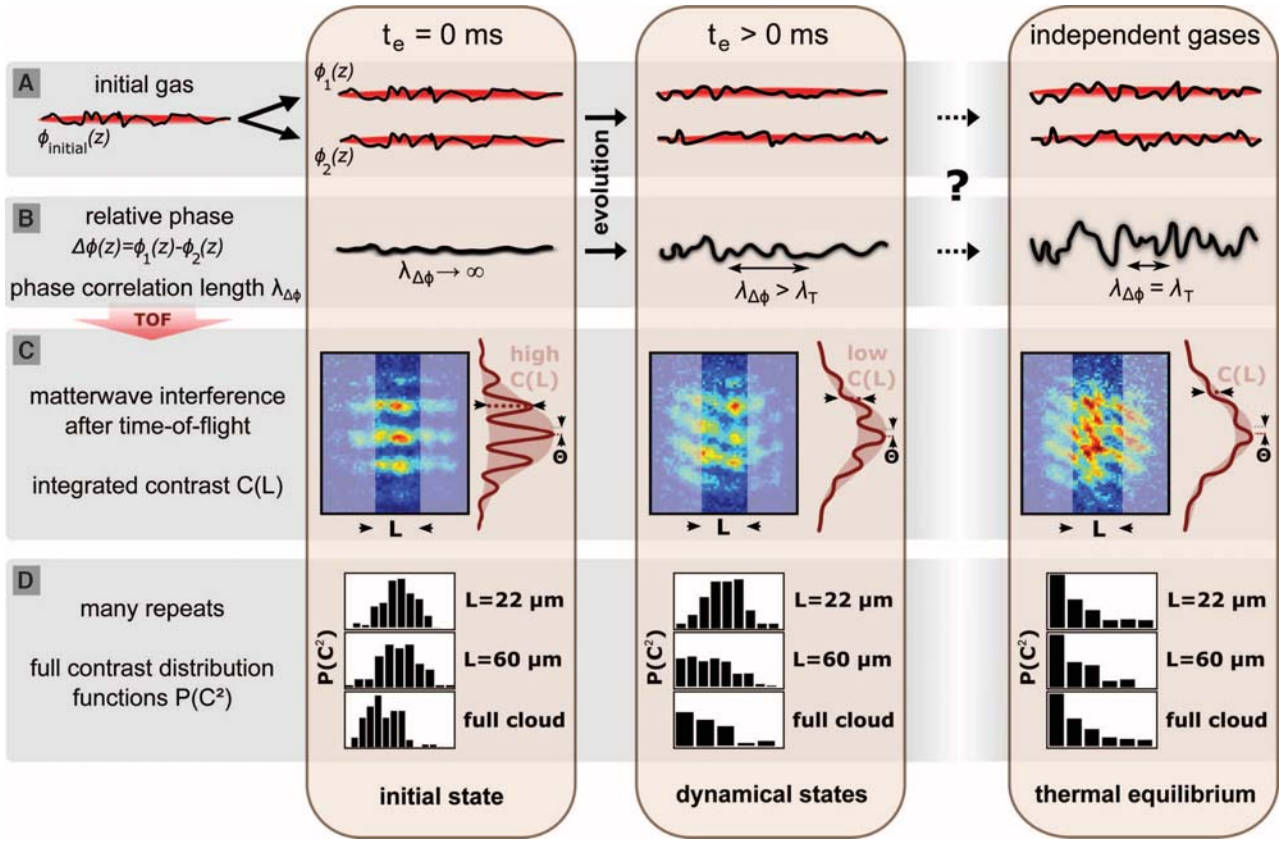

Fig. 1. (**A**) An initial-phase fluctuating 1D Bose gas is split into two uncoupled gases with almost identical phase distributions $\phi_1(z)$ and $\phi_2(z)$ (black solid lines) and allowed to evolve for a time t_e. (**B**) At t_e = 0 ms, fluctuations in the local phase difference $\Delta\phi(z)$ between the two gases are very small, and the corresponding phase correlation length is very large. During the evolution, these relative-phase fluctuations increase, and the correlation length decreases. The main question we address is whether or when this system will reach the corresponding thermal equilibrium of uncorrelated phases as characterized by the initial temperature T and thermal coherence length λ_T. In experiment, this situation can be prepared on purpose by splitting a thermal gas and cooling it into two independent gases (*32*). (**C**) Typical experimental matter-wave interference patterns obtained by overlapping the two gases in time-of-flight after different evolution times. Differences in the local relative phase lead to a locally displaced interference pattern. Integrated over a length L, the contrast $C(L)$ is a direct measure of the strength of the relative-phase fluctuations. (**D**) Because of the stochastic nature of the phase distributions, repeated experimental runs yield a characteristic distribution $P(C^2)$ of contrasts, which allows one to distinguish between the initial state, an intermediate prethermalized state, and the true thermal equilibrium of the system.

thermal equilibrium, if present at all, is expected to occur on a much longer time scale. It is conjectured that prethermalized states can be described by equilibrium statistical mechanics through a generalized Gibbs ensemble (*1*, *3*, *10*). Here, we present a direct observation of such a state.

Systems of ultracold atoms provide exceptional opportunities to experimentally study such nonequilibrium problems because of their almost perfect isolation from the environment. Moreover, the time scales for internal relaxation processes (collisions) are easily accessible in experiments. Consequently, there recently have been various studies about nonequilibrium dynamics in ultracold atom systems (*11*–*16*).

One-dimensional (1D) Bose gases are of particular interest because they inherently contain strong fluctuations and dynamics: At finite temperature, many longitudinal modes of the system are populated, which manifests itself in the rich spatial structure and dynamics in their local phase. This is in stark contrast with 3D condensates, in which the existence of long-range order allows the characterization of the state with a single, global phase. In addition, a homogeneous 1D Bose gas is a prime example of an integrable quantum system (*17*). Approximately realizing such systems in the experiment thus opens up the possibility of studying dynamics and relaxation close to an integrable point.

In our experiment (Fig. 1), we started from a single 1D Bose gas of ^{87}Rb in the quasi-condensate regime (*18*) prepared in an elongated microtrap on an atom chip (*19*). We prepared the initial state for our evolution by rapidly and coherently splitting the single 1D gas, producing a system of two uncoupled 1D Bose gases in a double-well potential. The two trapped 1D gases only differ by the quantum shot-noise introduced in the splitting (Figs. 1A); they have almost identical longitudinal phase profiles. In contrast, two independently created quasi-condensates have vastly different and uncorrelated phase profiles (Fig. 1, right column). The strongly correlated phase of the two gases after splitting reflects the memory that they originally come from a single quasi-condensate. Our experiment studies how this memory about the initial state evolves and decays in time and whether a thermal equilibrium state corresponding to two independent and classically separated quasi-condensates is reached in the evolution.

We probed the evolution of the local phase difference between the two quasi-condensates by using matter-wave interference (Fig. 1C). The system is allowed to evolve in the double-well for some evolution time t_e before the two 1D gases are released from the trap and allowed to interfere in time-of-flight. The local phase difference along the axial length of the system directly translates to a shift of the interference peaks along the transverse direction of the gases (Fig. 1C). To probe the strength of the fluctuations in the local phase difference $\Delta\phi(z)$, we integrated the interference pattern longitudinally over a variable length L and extracted from the resultant line profile our main experimental observable: the integrated contrast $C(L)$ (Fig. 1C). For the initial state, the local phase difference is close to zero everywhere along the quasi-condensates, and thus, the integrated interference contrast $C(L)$ is large for all integration lengths L. During the course of the evolution, the phase difference varies in the longitudinal direction as a result of the strong fluctuations inherent in 1D systems, which causes the reduction of $C(L)$, starting with long integration lengths. Thus, the measurements of $C(L)$ allow the characterization of the particular dynamics of 1D quasi-condensates.

The mean squared contrast $\langle C(L)^2 \rangle$, similarly to the coherence factor used in (*11*), is a direct measure of the integrated two-point correlation function of the relative phase between the two halves of the system (*20*, *21*). Integrating over the whole length of the interference pattern, we observed (Fig. 2A) an initial rapid decay in $\langle C^2 \rangle$ on a time scale of ~10 ms, after which a quasi-steady state emerges that slowly evolves further on a much slower time scale.

The initial rapid decay in Fig. 2A is analogous to the one observed in the experiment presented in (*12*), which was limited to $t_e < 12$ ms by longitudinal dynamics introduced in the splitting. Substantial improvements in the experimental techniques (*22*) allowed us to reveal the long-time behavior. We will first show that this steady state is not the expected thermal equilibrium and associate it with prethermalization (*4*).

To probe the nature of this quasi-steady state, we started by using tools developed to characterize equilibrium systems (*20*, *21*, *23*, *24*) and capture higher-order correlations in the system through the higher moments $\langle C^{2n} \rangle$. For this, we extracted

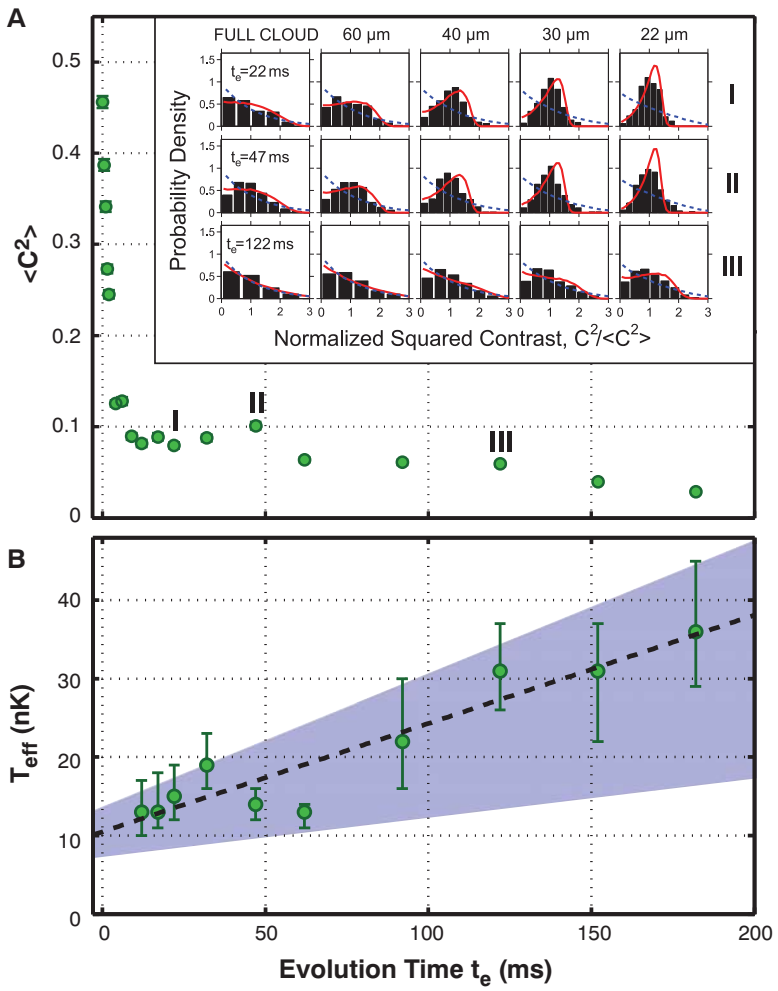

Fig. 2. (**A**) Evolution of the mean squared-contrast $\langle C^2 \rangle$ for interference patterns integrated over the whole length of the 1D systems. Rapid decay is followed by a long slow further evolution. Error bars are SEs of the mean. (Inset) Experimental nonequilibrium distributions of $C^2/\langle C^2 \rangle$ at t_e = 22, 47, and 122 ms, respectively (histograms) and a fit of a theoretical equilibrium distributions leading to $T_{eff} = 15^{+4}_{-3}$, 14^{+2}_{-2}, and 31^{+5}_{-6} nK, respectively (red solid line). For comparison, the calculated equilibrium distributions for T = 78 ± 10 nK (blue dashed line) are added. (**B**) Evolution of T_{eff} for the whole data set extracted by fitting equilibrium distributions. A linear fit indicates an increase of T_{eff} over time of 0.14 ± 0.04 nK/ms. The shaded area indicates the measured heating rate of our atom trap of 0.11 ± 0.06 nK/ms.

the full quantum mechanical probability distribution function (FDF) $P(C^2)dC^2$, which gives the probability to observe a value C^2 in the interval between C^2 and $C^2 + dC^2$. The higher moments $\langle C^{2n}\rangle$ are directly related to $P(C^2)$ by $\langle C^{2n}\rangle = \int C^{2n} P(C^2) dC^2$. Consequently, the FDF is a direct measure of all even relative-phase correlations between the gases and hence determines the state of the system in detail (*20*, *21*). In particular, high phase coherence between the two halves of the system results in a peaked Gumbel-like distribution, whereas the distribution is exponential in form when the phase coherence is low (*20*, *21*, *23*, *24*).

Using a statistically large set of data, we were able to map the time evolution of the FDFs for different length scales L. For times >12 ms—directly after the initial rapid evolution shown in Fig. 2A—we found remarkable agreement of the measured FDFs with theoretical equilibrium distributions. We extracted an effective temperature T_{eff} from a simultaneous fit to the measured data on all length scales probed (Fig. 2A, insets). Surprisingly, immediately after the fast decay at t_e = 12, 17, and 22 ms we found $T_{eff} = 13^{+4}_{-3}$, 13^{+5}_{-2}, and 15^{+4}_{-3} nK, respectively, which is roughly a factor of five lower than the initial temperature of the unsplit system (T = 78 ± 10 nK). The observed steady-state hence cannot be the true thermal equilibrium state of the system. For a direct comparison of the FDFs of the nonequilibrium system with the FDFs of a thermal equilibrium system, see (*22*). The interference is sensitive only to the relative degrees of freedom. The initial thermal energy remains stored in the common mode fluctuations of the two halves of the system, which are not probed by the interference pattern.

In contrast, for t_e < 12 ms the shapes of the measured FDFs were not consistent with equilibrium theory. The thermal-like appearance of the state is established only during the evolution of the system.

To analyze the subsequent further slow evolution observed in Fig. 2A, we extracted the effective temperature T_{eff} for all times after the initial decay (Fig. 2B). We found an increase of T_{eff} over time of 0.14 ± 0.04 nK/ms. This is, however, consistent with the measured heating rate of

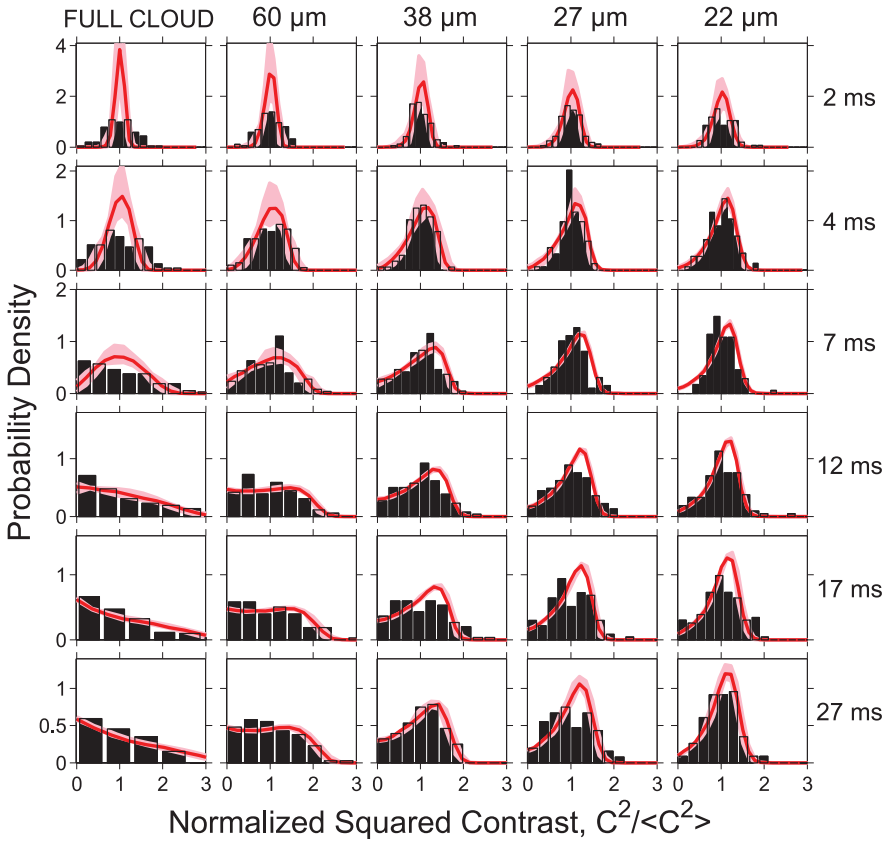

Fig. 3. The evolution of the squared-contrast distribution $P(C^2)$ for different integration lengths L. Experimental data are plotted by using histograms and the theoretical simulations as (red) curves. For integration over the full cloud length, the distribution rapidly becomes exponential with increasing evolution time t_e. For the shortest integration length, the distribution preserves a nonzero peak, showing a persisting memory of the correlations of the initial state (*33*). The light (pink) shaded areas denote the errors of the experimentally measured theory input parameters.

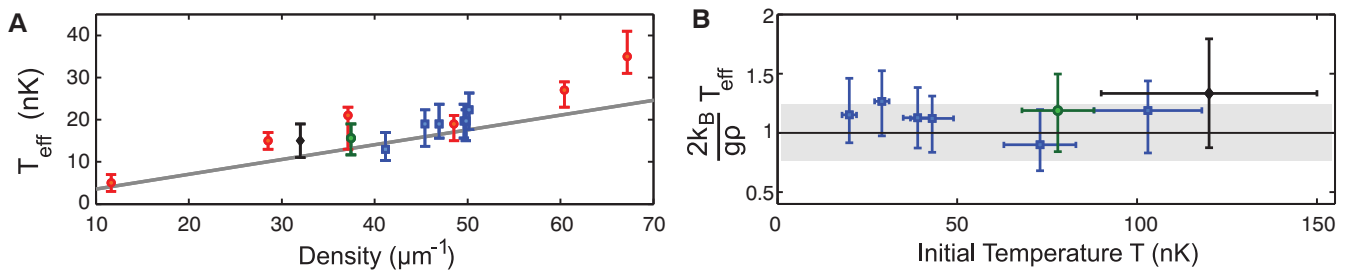

Fig. 4. (**A**) Dependence of T_{eff} on ρ and (**B**) independence of T_{eff} from the initial temperature T of the system before splitting, corrected for the scaling of T_{eff} with density. The colors encode different data sets. The (black) solid line corresponds to the theoretical prediction $k_B T_{eff} = g\rho/2$. In (A) and (B), the black data point corresponds to the data set presented in Fig. 3, and the green data point corresponds to the data set presented in Fig. 2.

our atom trap of 0.11 ± 0.06 nK/ms, which we characterized independently using equilibrium quasi-condensates (*22*). This indicates that either no thermalization is present in this nearly integrable system or, if it is present, that it is a very slow process.

To describe the fast evolution from the splitting to the emergence of the quasi-steady state, we used a fully integrable theory based on a Tomonaga-Luttinger liquid formalism (*22*, *25*, *26*). The evolution of the local phase difference between the two halves of the system $\Delta\phi(z)$ is described by a set of uncoupled collective modes with momentum k—that is, sound waves, which modulate the relative density and phase at a wavelength $\lambda = 2\pi/k$ and with an amplitude given by the population of the mode. A sudden splitting creates an equipartition of energy between all the k modes, which initially are all in phase (*22*). The rapid evolution of the system seen over the first ~10 ms corresponds to the dephasing of these k modes. The FDFs calculated by this integrable theory (*25*, *26*), by using input parameters independently extracted from the experiment, show agreement without any free parameter (Fig. 3).

The model also predicts a steady state to which the integrable system will relax: The dephasing, along with the equipartition of energy between the k modes introduced by the fast splitting, results in the FDFs of the quasi-steady state being indistinguishable from those of a system in thermal equilibrium at some effective temperature T_{eff}, which is determined by the energy given to the relative degrees of freedom by the quantum shot noise introduced in the splitting. The full calculation gives (*26*)

$$k_{\mathrm{B}} T_{\mathrm{eff}} = g\rho/2 \qquad (1)$$

where $g = 2\hbar\omega_{\perp}a_{\mathrm{s}}$ is the 1D interaction strength for particles with scattering length a_{s} trapped in a tube with transversal confinement $\omega_{\perp}$, ρ is the 1D density of each half of the system, and k_{B} is the Boltzmann constant. For the parameters used in the data presented in Fig. 3, the model predicts T_{eff} = 11 ± 3 nK, which is in good agreement with our observations of T_{eff} = 14 ± 4, 17 ± 5, and 14 ± 4 nK for the evolution times of 12, 17, and 27 ms, respectively.

Moreover, our integrable model predicts (Eq. 1) that the effective temperature should be linearly dependent on the initial 1D density and independent of the initial temperature. Both of these predictions are confirmed by extending the experiments over a wide range of initial conditions (Fig. 4).

The apparent systematic offset of the experimentally derived T_{eff} and the theoretical prediction in Fig. 4, A and B, can be attributed to imperfections in the experimental splitting process, which the model assumes to be instantaneous. This finite-time splitting is also the reason that the agreement between the experiment and theory in Fig. 3 is worse for very early times.

Nevertheless, the first milliseconds of the observed dynamics are well captured by the integrable Luttinger liquid theory. The large number of conserved quantities in this integrable system prevents thermalization. Our experimental realization of a 1D system is, however, not completely integrable and will eventually thermalize.

Dynamics beyond the harmonic Luttinger Liquid model is required to couple symmetric and antisymmetric modes and give rise to thermalization (*27*). A mechanism that is expected to come into play is interactions of particles that go beyond two-body collisions, such as three-body processes connected with higher radial trapping states (*28*–*30*). In our present experiment, these processes that can lead to full thermalization are much slower than the dephasing of the collective modes and thus allow the clear observation of the dynamics dominated by the close-by integrable system. It is of great interest to investigate the physics of thermalization in the future and study, for example, how far away from integrability one has to go to see full thermalization and probe its time scale.

In view of our present analysis, the observed decay of the coherence factor in the experiment of Hofferberth *et al*. (*12*) has to be reinterpreted. In agreement with our present experiment, it shows the same fast "integrable" dephasing of relative modes in the split 1D system (*25*, *26*, *31*) and not full decoherence and thermalization as originally interpreted by comparison with the theoretical description of Burkov *et al*. (*22*, *27*). For the present experiment, even independent of our theoretical model, the observed independence of T_{eff} from the initial temperature provides direct experimental evidence that we do not observe thermalization.

The quasi-steady state found in our experiments is not the thermal equilibrium state; nevertheless, it can be described by using an equilibrium model (*23*). It establishes on a time scale much shorter than the expected thermalization time and furthermore exhibits the properties of the dephased state of the corresponding integrable model (*26*). We thus conclude that our experiments provide a direct observation of prethermalization, as it is predicted to appear in nonequilibrium systems close to an integrable point (*10*). That the effective temperature is independent from the kinetic temperature supports the prediction that such a state requires a description by a generalized Gibbs ensemble (*1*, *3*, *10*).

Our experiment also directly shows that the two separated many-body systems retain memory of their initial state for a time much longer than the randomization of the global phase would suggest, and that genuine decoherence that would erase the memory did not yet occur—that is, the two 1D systems did not yet emerge as two classically separated entities.

The time scale over which this prethermalized state persists remains an open question. It is directly related to the open problems of how two quantum-mechanically entangled objects reach classicality, the properties of the hypothetical quantum Kolmogorov-Arnold-Moser theorem (*1*), and the very nature of thermalization itself.

References and Notes

1. A. Polkovnikov, K. Sengupta, A. Silva, M. Vengalattore, *Rev. Mod. Phys.* **83**, 863 (2011).
2. S. Goldstein, J. L. Lebowitz, R. Tumulka, N. Zanghì, *Eur. Phys. J. H* **35**, 173 (2010).
3. M. Rigol, V. Dunjko, M. Olshanii, *Nature* **452**, 854 (2008).
4. J. Berges, S. Borsányi, C. Wetterich, *Phys. Rev. Lett.* **93**, 142002 (2004).
5. C. Kollath, A. M. Läuchli, E. Altman, *Phys. Rev. Lett.* **98**, 180601 (2007).
6. M. Eckstein, M. Kollar, P. Werner, *Phys. Rev. Lett.* **103**, 056403 (2009).
7. M. Moeckel, S. Kehrein, *N. J. Phys.* **12**, 055016 (2010).
8. L. Mathey, A. Polkovnikov, *Phys. Rev. A* **81**, 033605 (2010).
9. R. Barnett, A. Polkovnikov, M. Vengalattore, *Phys. Rev. A* **84**, 023606 (2011).
10. M. Kollar, F. A. Wolf, M. Eckstein, *Phys. Rev. B* **84**, 054304 (2011).
11. T. Kinoshita, T. Wenger, D. S. Weiss, *Nature* **440**, 900 (2006).
12. S. Hofferberth, I. Lesanovsky, B. Fischer, T. Schumm, J. Schmiedmayer, *Nature* **449**, 324 (2007).
13. L. E. Sadler, J. M. Higbie, S. R. Leslie, M. Vengalattore, D. M. Stamper-Kurn, *Nature* **443**, 312 (2006).
14. S. Ritter *et al*., *Phys. Rev. Lett.* **98**, 090402 (2007).
15. A. Widera *et al*., *Phys. Rev. Lett.* **100**, 140401 (2008).
16. S. Trotzky *et al*., *Nat. Phys.* **8**, 325 (2012).
17. E. H. Lieb, W. Liniger, *Phys. Rev.* **130**, 1605 (1963).
18. K. V. Kheruntsyan, D. M. Gangardt, P. D. Drummond, G. V. Shlyapnikov, *Phys. Rev. Lett.* **91**, 040403 (2003).
19. J. Reichel, V. Vuletic, Eds., *Atom Chips* (Wiley VCH, New York, 2011).
20. A. Polkovnikov, E. Altman, E. Demler, *Proc. Natl. Acad. Sci. U.S.A.* **103**, 6125 (2006).
21. V. Gritsev, E. Altman, E. Demler, A. Polkovnikov, *Nat. Phys.* **2**, 705 (2006).
22. Materials and methods are available as supplementary materials on *Science* Online.
23. H.-P. Stimming, N. J. Mauser, J. Schmiedmayer, I. E. Mazets, *Phys. Rev. Lett.* **105**, 015301 (2010).
24. S. Hofferberth *et al*., *Nat. Phys.* **4**, 489 (2008).
25. T. Kitagawa *et al*., *Phys. Rev. Lett.* **104**, 255302 (2010).
26. T. Kitagawa, A. Imambekov, J. Schmiedmayer, E. Demler, *New J. Phys.* **13**, 073018 (2011).
27. A. A. Burkov, M. D. Lukin, E. Demler, *Phys. Rev. Lett.* **98**, 200404 (2007).
28. I. E. Mazets, T. Schumm, J. Schmiedmayer, *Phys. Rev. Lett.* **100**, 210403 (2008).
29. I. E. Mazets, J. Schmiedmayer, *New J. Phys.* **12**, 055023 (2010).
30. S. Tan, M. Pustilnik, L. I. Glazman, *Phys. Rev. Lett.* **105**, 090404 (2010).
31. R. Bistritzer, E. Altman, *Proc. Natl. Acad. Sci. U.S.A.* **104**, 9955 (2007).
32. S. Hofferberth, I. Lesanovsky, B. Fischer, J. Verdu, J. Schmiedmayer, *Nat. Phys.* **2**, 710 (2006).
33. M. Olshanii *et al*., *Nat. Comput.* **3**, 641 (2012).

Acknowledgments: We thank Ch. v. Hagen and M. Göbel for early work on the experimental apparatus and the Vienna group for invaluable discussions and assistance. The atom chip was fabricated at ZMNS, TU Wien by W. Schrenk and M. Trinker. The experiments were supported by the Austrian Science Fund (FWF) through grants P22590-N16 and M1040-N16, the Doctoral Programme CoQuS (W1210), grant

P22590-N16 and the Wittgenstein Prize, and the European Union through the integrating project AQUTE, Siemens Austria, and the City of Vienna. T.K. and E.D. thank the Army Research Office for funding from the Defense Advanced Research Projects Agency Optical Lattice Emulator program, Harvard-MIT CUA, NSF grant DMR-07-05472, Air Force Office of Scientific Research Quantum Simulation Multidisciplinary University Research Initiative (MURI), and the Army Research Office–MURI on Atomtronics.

Supplementary Materials
www.sciencemag.org/cgi/content/full/science.1224953/DC1
Materials and Methods
Supplementary Text
Figs. S1 to S5
References (*34*–*58*)

21 May 2012; accepted 21 August 2012
Published online 6 September 2012;
10.1126/science.1224953

Oxidative Aliphatic C-H Fluorination with Fluoride Ion Catalyzed by a Manganese Porphyrin

Wei Liu,[1] Xiongyi Huang,[1] Mu-Jeng Cheng,[2] Robert J. Nielsen,[2] William A. Goddard III,[2] John T. Groves[1]*

Despite the growing importance of fluorinated organic compounds in drug development, there are no direct protocols for the fluorination of aliphatic C-H bonds using conveniently handled fluoride salts. We have discovered that a manganese porphyrin complex catalyzes alkyl fluorination by fluoride ion under mild conditions in conjunction with stoichiometric oxidation by iodosylbenzene. Simple alkanes, terpenoids, and even steroids were selectively fluorinated at otherwise inaccessible sites in 50 to 60% yield. Decalin was fluorinated predominantly at the C2 and C3 methylene positions. Bornyl acetate was converted to exo-5-fluoro-bornyl acetate, and 5α-androstan-17-one was fluorinated selectively in the A ring. Mechanistic analysis suggests that the regioselectivity for C-H bond cleavage is directed by an oxomanganese(V) catalytic intermediate followed by F delivery via an unusual manganese(IV) fluoride that has been isolated and structurally characterized.

Biochemistry manifests numerous highly selective transformations of aliphatic C-H bonds into alcohols, halides, and olefins catalyzed by reactive metal-oxo intermediates within enzymes (*1*, *2*). A notable exception is aliphatic C-H bond fluorination: The only fluorinase enzymes yet characterized form C-F bonds by nucleophilic displacement at the preactivated C center of *S*-adenosylmethionine (*3*, *4*). There are no catalytic ways to selectively and directly incorporate fluoride ions into unreactive sp^3 C-H bonds. Yet there is an enormous impetus today to place F at such inaccessible sites in biomolecules and drug candidates. Fluorination of drugs can block sites of phase I metabolism by cytochrome P450 enzymes as well as improving target-binding affinities (*5*). Further, the incorporation of ^{18}F into biomolecules can allow direct imaging of metabolic activity and drug targets using the exquisite sensitivity of positron emission tomography (*6*, *7*).

Although strategies for aromatic fluorination developed over the past 5 years have provided access to complex aryl fluorides (*8*–*11*), there has been a notable lack of recent progress in the catalytic fluorination of aliphatic C-H bonds (*12*–*14*). Direct C-H fluorination with elemental F and electrophilic fluorinating agents, as developed by Rozen, Sandford, and Chambers (*15*–*17*), are viable and very useful methods. Metal-catalyzed direct benzylic C-H fluorination has been achieved recently with palladium catalysts and an "F^+" source (*18*). Also, advances in organocatalytic fluorination have enabled enantioselective formation of C-F bonds adjacent to a carbonyl group (*19*) or to an alcohol, in the latter case via the ring-opening of epoxides with a fluoride nucleophile (*20*). A chemo-enzymatic fluorination strategy via initial P450-mediated hydroxylation (*21*) and chemical routes involving initial decarboxylation (*22*, *23*) have also been reported. Despite this impressive progress, a method for the selective and efficient incorporation of F at unactivated C-H sites within a target molecule using fluoride ion is singularly absent from the repertoire of chemical synthesis.

The paradoxical challenge of achieving selective aliphatic fluorination lies in discovering a catalyst that is both sufficiently reactive and predictably selective to transform these ubiquitous yet unactivated sp^3 C-H bonds in the presence of other common functional groups. Such a catalyst would be particularly useful if it could use fluoride ion under convenient laboratory conditions. A strategy was suggested to us by our recent discovery of a C-H chlorination protocol using manganese porphyrin catalysts and hypochlorite ion (*24*). We considered that site-selective fluorination might be achieved if a suitable fluoride source could be found that redirected the usual biomimetic O rebound scenario (*2*) to metal-bound fluoride, in the manner of halogenating metalloenzymes such as SyrB2 that generate an oxo-chloroferrate intermediate (*25*). Thus, could a manganese fluoride capture substrate radicals generated by oxomanganese-mediated H abstraction? We report here a successful manganese-catalyzed oxidative C-H bond fluorination using fluoride ion.

We have found that a variety of simple alkanes and substituted alkanes, as well as larger natural-product molecules, can be fluorinated effectively in the presence of catalytic amounts of the bulky manganese porphyrin Mn(TMP)Cl (**1**). This oxidative aliphatic fluorination reaction is driven by iodosylbenzene as the oxo-transfer agent, using silver fluoride/tetrabutylammonium fluoride trihydrate as the fluoride source, both in stoichiometric excess (*26*). Ultra-dry conditions are not required. Results for the initial exploratory reactions of a panel of simple substrates are presented in Table 1. Cycloalkanes afforded monofluorinated products in ~50% yield. Typically, conversions were ~70%, with small amounts (15 to 20%) of alcohols and ketones also being produced. No products were detected in control experiments that omitted the manganese porphyrin or iodosylbenzene, whereas a ~2:1 ratio of oxygenated to fluorinated products was formed in the absence of tetrabutylammonium fluoride. Only oxygenated products were formed without silver fluoride (*27*). There were negligible amounts of difluorides produced at this level of conversion, probably due to the electron deficiency of the products induced by the F atom (*28*). A preliminary investigation of the substrate scope led to the results shown in Table 1 (entries 7 to 12). A range of substituted molecules, including ester, tertiary alcohol, ketone, and amide substituents, proved to be good substrates for fluorination with catalyst **1**. Fluorination of methyl cyclohexylcarboxylate (entry 7) and methyl cyclohexanol (entry 8) afforded *trans*-C3 fluorides as the major products. Monosubstituted five- and seven-membered cycloalkanes (entries 9, 10, and 12) were fluorinated exclusively at the C3 and C4 positions, respectively, suggesting subtle stereoelectronic effects on the selectivity of this reaction.

Having demonstrated that it is possible to redirect manganese-catalyzed hydroxylation to fluorination, we next aimed to apply this reaction to larger molecules. The reaction of *trans*-decalin under the same conditions afforded methylene monofluorination products with a 3.5-to-1 preference for C2 over C1 in an overall 51% yield and a 75% conversion (Fig. 1A). Very high methylene regioselectivity was observed for this substrate (>95%), similar to that observed for the manganese-catalyzed chlorination reaction we have

[1]Department of Chemistry, Frick Chemistry Laboratory, Princeton University, Princeton, NJ 08544, USA. [2]Department of Chemistry, Materials and Process Simulation Center (MC 139-74), California Institute of Technology, Pasadena, CA 91125, USA. *To whom correspondence should be addressed. E-mail: jtgroves@princeton.edu